THE JOURNAL OF BIOLOGICAL CHEMISTRY VOL. 283, NO. 16, pp. 10892–10903, April 18, 2008
Printed in the U.S.A.

Mitochondrial Autophagy Is an HIF-1-dependent Adaptive Metabolic Response to Hypoxia*[S]

Received for publication, January 4, 2008, and in revised form, February 8, 2008 Published, JBC Papers in Press, February 15, 2008, DOI 10.1074/jbc.M800102200

Huafeng Zhang[‡§], Marta Bosch-Marce[‡§], Larissa A. Shimoda[¶], Yee Sun Tan[‡§], Jin Hyen Baek[‡§], Jacob B. Wesley[‡§], Frank J. Gonzalez[‖], and Gregg L. Semenza[‡§¶‡‡§§1]**

*From the [‡]Vascular Program, Institute for Cell Engineering, [§]McKusick-Nathans Institute of Genetic Medicine, and [¶]Department of Medicine, **Pediatrics, [‡‡]Oncology, and [§§]Radiation Oncology, The Johns Hopkins University School of Medicine, Baltimore, Maryland 21205 and [‖]Laboratory of Metabolism, NCI, National Institutes of Health, Bethesda, Maryland 20892*

Autophagy is a process by which cytoplasmic organelles can be catabolized either to remove defective structures or as a means of providing macromolecules for energy generation under conditions of nutrient starvation. In this study we demonstrate that mitochondrial autophagy is induced by hypoxia, that this process requires the hypoxia-dependent factor-1-dependent expression of BNIP3 and the constitutive expression of Beclin-1 and Atg5, and that in cells subjected to prolonged hypoxia, mitochondrial autophagy is an adaptive metabolic response which is necessary to prevent increased levels of reactive oxygen species and cell death.

The survival of metazoan organisms is dependent upon their ability to efficiently generate energy through the process of mitochondrial oxidative phosphorylation in which reducing equivalents, derived from the oxidation of acetyl CoA in the tricarboxylic acid cycle, are transferred from NADH and $FADH_2$ to the electron transport chain and ultimately to O_2, a process which produces an electrochemical gradient that is used to synthesize ATP (1). Although oxidative phosphorylation is more efficient than glycolysis in generating ATP, it carries the inherent risk of generating reactive oxygen species (ROS)[2] as a result of electrons prematurely reacting with O_2 at respiratory complex I or complex III. Transient, low level ROS production is utilized for signal transduction in metazoan cells, but prolonged elevations of ROS result in the oxidation of protein, lipid, and nucleic acid leading to cell dysfunction or death. O_2 delivery and utilization must, therefore, be precisely regulated to maintain energy and redox homeostasis.

Hypoxia-inducible factor 1 (HIF-1) plays a key role in the regulation of oxygen homeostasis (2, 3). HIF-1 is a heterodimer composed of a constitutively expressed HIF-1β subunit and an O_2-regulated HIF-1α subunit (4). Under aerobic conditions, HIF-1α is hydroxylated on proline residue 402 and/or 564 by prolyl hydroxylase 2 a dioxygenase that utilizes O_2 and α-ketoglutarate as co-substrates with ascorbate as co-factor in a reaction that generates succinate and CO_2 as side products (5–8). Under hypoxic conditions the rate of hydroxylation declines, either as a result of inadequate substrate (O_2) or as a result of hypoxia-induced mitochondrial ROS production, which may oxidize Fe(II) in the catalytic center of the hydroxylase (9, 10). Hydroxylated HIF-1α is bound by the von Hippel-Lindau protein, which recruits a ubiquitin protein ligase complex that targets HIF-1α for proteasomal degradation (11–14).

HIF-1 regulates the transcription of hundreds of genes in response to hypoxia (15, 16), including the *EPO* (17) and *VEGF* (18) genes that encode proteins required for erythropoiesis and angiogenesis, respectively, which serve to increase O_2 delivery. In addition, HIF-1 controls a series of molecular mechanisms designed to maintain energy and redox homeostasis. First, HIF-1 coordinates a switch in the composition of cytochrome *c* oxidase (mitochondrial electron-transport chain complex IV) from COX4-1 to COX4-2 subunit utilization, which increases the efficiency of cytochrome *c* oxidase under hypoxic conditions (19). Second, HIF-1 activates transcription of the *PDK1* gene encoding a kinase that phosphorylates and inactivates pyruvate dehydrogenase, thereby shunting pyruvate away from the mitochondria by preventing its conversion to acetyl CoA (20, 21). Third, HIF-1 activates transcription of genes encoding glucose transporters and glycolytic enzymes to increase flux from glucose to lactate (22–24). Fourth, HIF-1 represses mitochondrial biogenesis and respiration (25). Interference with the HIF-1-dependent regulation of mitochondrial respiration under conditions of prolonged hypoxia ($\geq$24 h) leads to increased ROS levels and increased apoptosis (18, 20, 25).

Mitochondria are replaced every 2–4 weeks in rat brain, heart, liver, and kidney (26). The destruction of mitochondria is believed to occur via the process of autophagy, in which parts of the cytoplasm, including organelles, are

* This work was supported by funds from the Johns Hopkins Institute for Cell Engineering and National Institutes of Health Public Health Service Grant P50-CA103175. The costs of publication of this article were defrayed in part by the payment of page charges. This article must therefore be hereby marked "*advertisement*" in accordance with 18 U.S.C. Section 1734 solely to indicate this fact.

[S] The on-line version of this article (available at http://www.jbc.org) contains supplemental Figs. 1–6 and Tables 1 and 2.

[1] To whom correspondence should be addressed: Broadway Research Bldg., Suite 671, 733 North Broadway, Baltimore, MD 21205. Fax: 443-287-5618; E-mail: gsemenza@jhmi.edu.

[2] The abbreviations used are: ROS, reactive oxygen species; HIF-1, hypoxia-inducible factor-1; MEF, mouse embryo fibroblast; WT, wild type; KO, knockout; HET, heterozygous-null; SNC, scrambled negative control short hairpin RNA; siRNA, small interfering RNA; MnTMPyP, Mn(III) tetrakis (1-methyl-4-pyridyl) porphyrin pentachloride; NAO, nonyl acridine orange; EV, empty vector; GFP, green fluorescent protein; 7-AAD, 7-aminoactinomycin D.

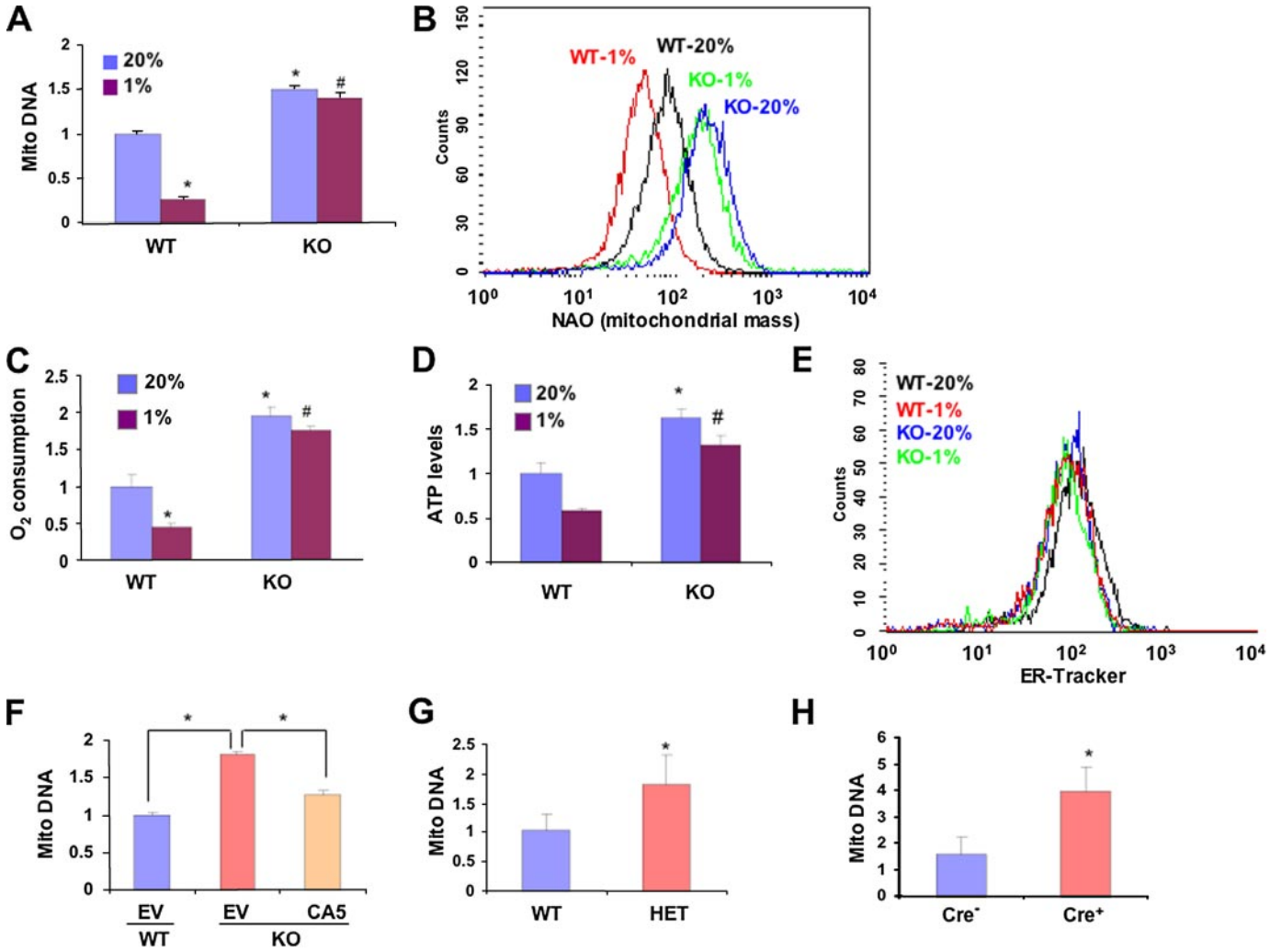

FIGURE 1. **Regulation of mitochondrial mass and respiration by HIF-1 *ex vivo* and *in vivo*.** *A*, the ratio of mitochondrial:nuclear DNA was determined by quantitative real-time PCR in wild type (*WT*) and *Hif1a*$^{-/-}$ (*KO*) MEFs exposed to 20 or 1% O_2 for 48 h and normalized to the results obtained for WT cells at 20% O_2. Mean values are shown (±S.E.). *, $p < 0.05$ by Student's *t* test compared with WT MEFs at 20% O_2; #, $p < 0.05$ compared with WT MEFs at 1% O_2. *B*, WT and KO MEFs were exposed to 20 or 1% O_2 for 48 h. Equal numbers of cells were stained with nonyl acridine orange (*NAO*) and analyzed by flow cytometry to measure mitochondrial mass. *C* and *D*, O_2 consumption (*C*) and ATP levels (*D*) were measured in WT and KO MEFs exposed to 20 or 1% O_2 for 48 h and normalized to the results obtained for WT MEFs at 20% O_2. Mean values are shown (±S.E.). *, $p < 0.05$ by Student's *t* test compared with WT MEFs at 20% O_2; #, $p < 0.05$ compared with WT MEFs at 1% O_2. *E*, WT and KO MEFs were exposed to 20 or 1% O_2 for 48 h. Equal numbers of cells were stained with ER-Tracker and analyzed by flow cytometry to measure endoplasmic reticulum mass. *F*, WT and KO MEFs were transduced with empty retroviral vector (*EV*) or vector encoding constitutively active HIF-1α (*CA5*). After 3 days the ratio of mitochondrial:nuclear DNA was determined. Mean values are shown (±S.E.). *, $p < 0.05$ for indicated comparison. *G* and *H*, DNA was isolated from lungs of WT and *Hif1a*$^{+/-}$ HIF-1α-HET littermate mice (*G*) or *Arnt*$^{flox/flox}$ HIF-1β-conditional-knock-out mice that were either transgenic (*Cre*$^{+}$) or non-transgenic (*Cre*$^{-}$) for *Tie2-Cre* (*H*). The ratio of mitochondrial: nuclear DNA was determined by real-time PCR and normalized to the results obtained for WT (*G*) or Cre^{-} (*H*) mice. *, mean (± S.E., $n = 3$) that is significantly different from WT or Cre^{-}.

sequestered in double-membrane autophagic vacuoles or autophagosomes (27, 28). In addition to providing a mechanism for disposing of damaged mitochondria, autophagy is induced by environmental stress stimuli such as nutrient deprivation (29, 30). Autophagy is induced in hearts subjected to hypoxic or ischemic conditions and has been proposed by various investigators to play either a protective or pathogenic role in heart disease (30–33).

We hypothesized that induction of mitochondrial autophagy, in concert with inhibition of mitochondrial biogenesis (25), represents a critical adaptive mechanism to maintain oxygen homeostasis under hypoxic conditions. To test this hypothesis, we performed experiments to establish conditions under which hypoxia was a sufficient stimulus to induce mitochondrial autophagy, to determine whether this response was HIF-1-dependent, and to investigate whether mitochondrial autophagy was specifically required for the maintenance of redox homeostasis and the survival of hypoxic cells.

EXPERIMENTAL PROCEDURES

Cell Culture—Wild type (WT) and *Hif1a*$^{-/-}$ knock-out (KO) mouse embryo fibroblasts (MEFs) were immortalized by SV40 large T antigen and maintained in high glucose (4.5 mg/ml) Dulbecco's modified Eagle's medium (Invitrogen) with 15% fetal bovine serum (Invitrogen), 2 mM sodium pyruvate (Sigma), nonessential amino acids (Sigma), and 1% penicillin-streptomycin (Invitrogen) (34). Cells were maintained at 37 °C in a 5% CO_2, 95% air incubator (20% O_2). Hypoxic cells (1% O_2)

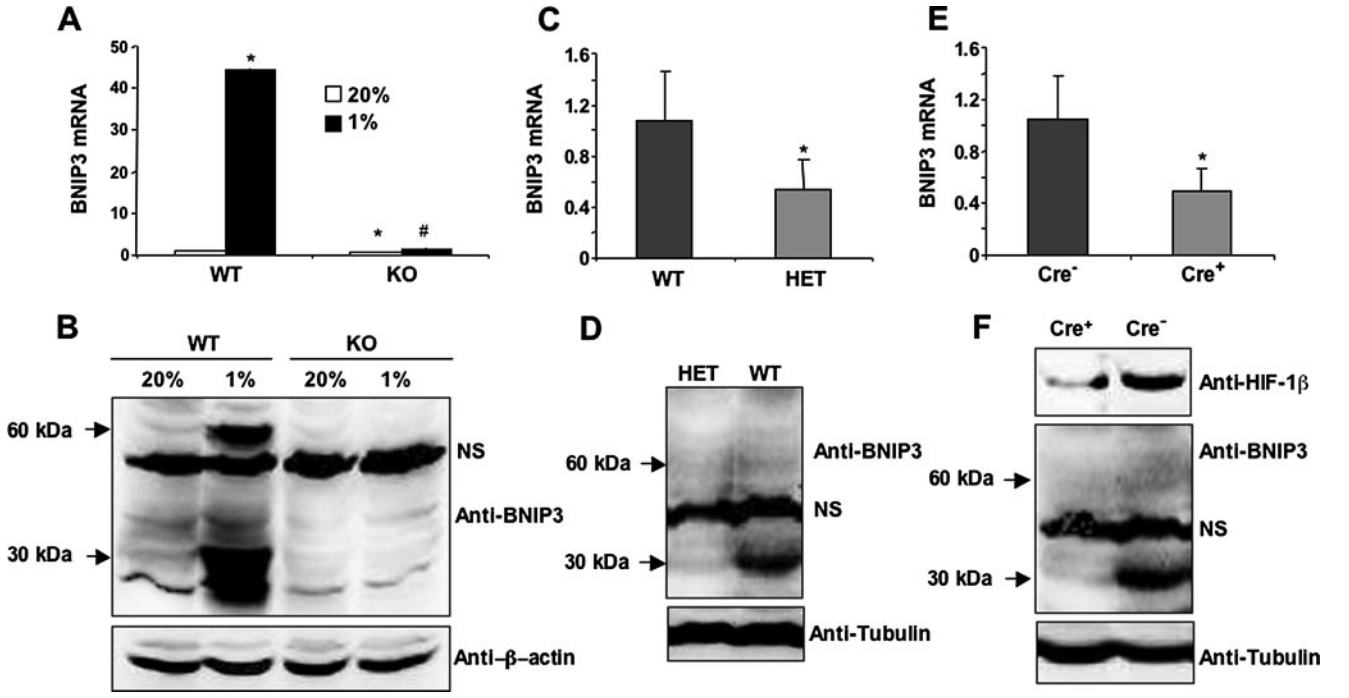

FIGURE 2. **HIF-1-dependent induction of BNIP3 expression in hypoxic MEFs.** *A*, BNIP3 mRNA was measured by quantitative real-time RT-PCR in WT and KO MEFs exposed to 20 or 1% O_2 for 24 h. Mean values (±S.E.) are shown. *, $p < 0.05$ by Student's *t* test compared with WT MEFs at 20% O_2; #, $p < 0.05$ compared with WT MEFs at 1% O_2. *B*, BNIP3 and β-actin protein expression was measured by immunoblot assay using lysates from WT and KO MEFs exposed to 20 or 1% O_2 for 48 h. *C* and *D*, BNIP3 mRNA (*C*) and protein (*D*) expression were analyzed in WT and HET mouse lung tissues. *, mean (±S.E., $n = 3$) that is significantly different from WT. Anti-tubulin immunoblot assay was performed to confirm equal protein loading. *E* and *F*, BNIP3 mRNA (*E*) and protein (*F*) levels were analyzed in Cre^- and Cre^+ mouse lung tissues. *, mean (±S.E., $n = 3$) that is significantly different from Cre^-. Tubulin served as loading control. *NS* indicates a nonspecific band.

were maintained in a modular incubator chamber flushed with a gas mixture containing 1% O_2, 5% CO_2, and 94% N_2 at 37 °C. For experiments involving hypoxia, all cells were maintained in culture media supplemented with 25 mM HEPES buffer.

Plasmids and Reagents—Mouse Beclin-1 cDNA was cloned into SalI/BamHI sites of plasmid 3xFLAG-CMV-7 (Sigma). Transfection into MEFs was performed using Lipofectamine Plus (Invitrogen) according to the manufacturer's instructions. MnTMPyP (Mn(III) tetrakis (1-methyl-4-pyridyl) porphyrin pentachloride) was purchased from Calbiochem.

Mouse Strains—WT and *Hif1a*$^{+/-}$ heterozygous-null (HET) mice were described previously (22). *Arnt*$^{flox/flox}$ mice with conditional knock-out of the *Arnt* gene encoding HIF-1β in endothelial cells were generated using the *Cre-loxP* system as described previously (35). 6–8-Week-old WT and HET or Cre^- and Cre^+ littermate mice were used.

Establishment of Stably Transfected Cell Lines—Retroviral vectors pQCXIP and pQCXIN (Clontech) encoding human BNIP3 or HIF-1αCA5 (15), respectively, were constructed and co-transfected with plasmids encoding group antigen, polymerase, envelope protein, and vesicular stomatitis virus G protein into 293T-packaging cells using FuGENE 6 (Roche Applied Science). Viral supernatant was collected 48 h post-transfection, filtered (0.45-μm pore size), and added to MEFs in the presence of 8 μg/ml Polybrene (Sigma-Aldrich). The transduced cells were selected by the addition of 1.5 μg/ml puromycin to establish stable subclones. Short hairpin RNA (shRNA) targeting BNIP3, corresponding to nucleotides 80–98 (sh80) or 82–100 (sh82) of GenBank™ accession number NM_009760, as well as shRNA targeting Beclin-1, corresponding to nucleotides 765–783 of GenBank™ accession number NM_019584 (supplemental Table S1), were inserted into the mammalian expression vector pSR.retro.puro (OligoEngine, Seattle, WA). WT-sh80, WT-sh82, WT-shBeclin, and KO-shBeclin stable cell lines were established by retrovirus infection followed by selection and maintenance in puromycin (1.5 and 1.0 μg/ml for WT and KO, respectively). The lentiviral FURW-Bcl-2 vector or FURW empty vector (provided by L. Cheng and R. Siliciano) was cotransfected with plasmids encoding vesicular stomatitis virus G and human immunodeficiency virus-1 *gag/pol*, *tat*, and *rev* proteins into 293T-packaging cells using FuGENE 6 (Roche Applied Science), and transduction was performed using the same procedure described above.

Mitochondrial DNA Copy Measurement—Total DNA was extracted from mouse tissues or MEFs. The amount of mitochondrial DNA relative to nuclear DNA was determined by quantitative real-time PCR using primers (supplemental Table S2) for *Nd2* (NADH dehydrogenase subunit 2; mitochondrial genome) and *Nme1* (nuclear genome). Relative *Nd2* copy number was calculated based on the threshold cycle (Ct) as $2^{-\Delta(\Delta Ct)}$, where $\Delta Ct = Ct_{Nd2} - Ct_{Nme1}$, and $\Delta(\Delta Ct) = \Delta Ct_{sample} - \Delta Ct_{control}$.

Immunoblot Analysis—Equal amounts of protein extracted from MEFs with radioimmune precipitation assay buffer were fractionated by 10% SDS-PAGE. Anti-BNIP3 (Abcam, Inc.), anti-FLAG (Sigma), anti-HIF-1α, anti-Bcl2, and anti-LC3 (Novus Biologicals, Inc.) antibodies were used for immunoblot

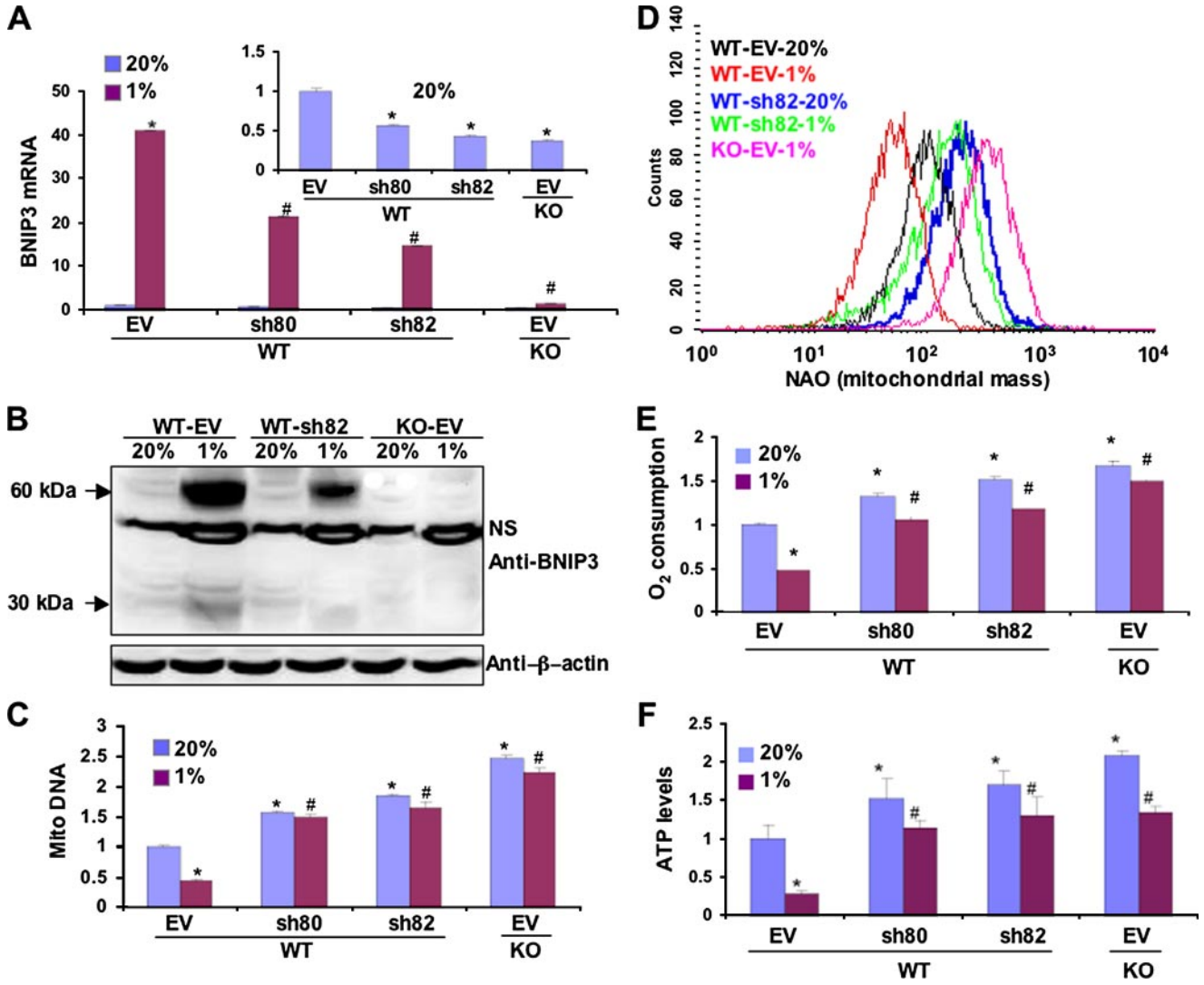

FIGURE 3. **Effect of BNIP3 loss-of-function on mitochondrial mass and respiration in WT and KO MEFs.** *A* and *B*, quantitative real-time RT-PCR (*A*) and immunoblot analysis (*B*) showed down-regulation of BNIP3 mRNA and protein, respectively, by short hairpin RNAs sh80 and sh82 in cells incubated at 20 or 1% O_2 for 24 h (*A*) or 48 h (*B*). β-Actin blot showed equal protein loading. *NS*, nonspecific band. *C*, *D*, *E*, and *F*, mitochondrial DNA content (*C*), mitochondrial mass (*D*), O_2 consumption (*E*), and ATP levels (*F*) were measured in MEF subclones that were stably transfected with EV or vector encoding sh80 or sh82 and cultured at 20 or 1% O_2 for 48 h. Data are presented as the mean (±S.E.). *, $p < 0.05$ by Student's *t* test compared with WT-EV MEFs at 20% O_2; #, $p < 0.05$ compared with WT-EV MEFs at 1% O_2.

assays. Blots were stripped and re-probed with β-actin or tubulin antibody to confirm equal protein loading.

Quantitative Real-time Reverse Transcription PCR—Total RNA was isolated using Trizol reagent (Invitrogen) followed by DNase (Ambion) treatment according to the manufacturer's instructions. One microgram of total RNA was used for first-strand cDNA synthesis using iScript cDNA Synthesis system (Bio-Rad). cDNA samples were diluted 1:10, and real-time PCR was performed using iQ SYBR Green Supermix and the iCycler real-time PCR detection system (Bio-Rad). Primers for BNIP3 and Beclin-1 were designed using Beacon Designer software (supplemental Table S2), and the annealing temperature was optimized by gradient PCR. The -fold change in expression of each target mRNA (BNIP3 or Beclin-1) relative to 18 S rRNA was calculated based on the threshold cycle (Ct) as $2^{-\Delta(\Delta Ct)}$, where $\Delta Ct = Ct_{target} - Ct_{18\,S}$, and $\Delta(\Delta Ct) = \Delta\, Ct_{sample} - \Delta Ct_{control}$.

Flow Cytometry—Mitochondrial mass, intracellular ROS levels, and endoplasmic reticulum mass were measured by staining cells with 10 nM nonyl acridine orange (NAO), 1 μM dichlorodihydrofluorescein diacetate, or 1 μM ER-tracker green dye (BODIPY® FL glibenclamide) (Molecular Probes), respectively, at 37 °C for 15 min in 5% fetal bovine serum, phosphate-buffered saline (PBS) solution, followed by washing with PBS. Stained cells were filtered and analyzed immediately with a FACScan flow cytometer (BD Bioscience). All gain and amplifier settings were held constant for the duration of the experiment. Apoptosis was measured by flow cytometry using the annexin V-PE apoptosis detection kit (BD Bioscience) according to the manufacturer's instructions.

Measurement of Cellular O_2 Consumption—Cells were trypsinized and suspended at 3×10^6 cells/ml in Dulbecco's modified Eagle's medium, 10% fetal bovine serum, and 25 mM HEPES buffer. For each set of experiments, equal numbers of

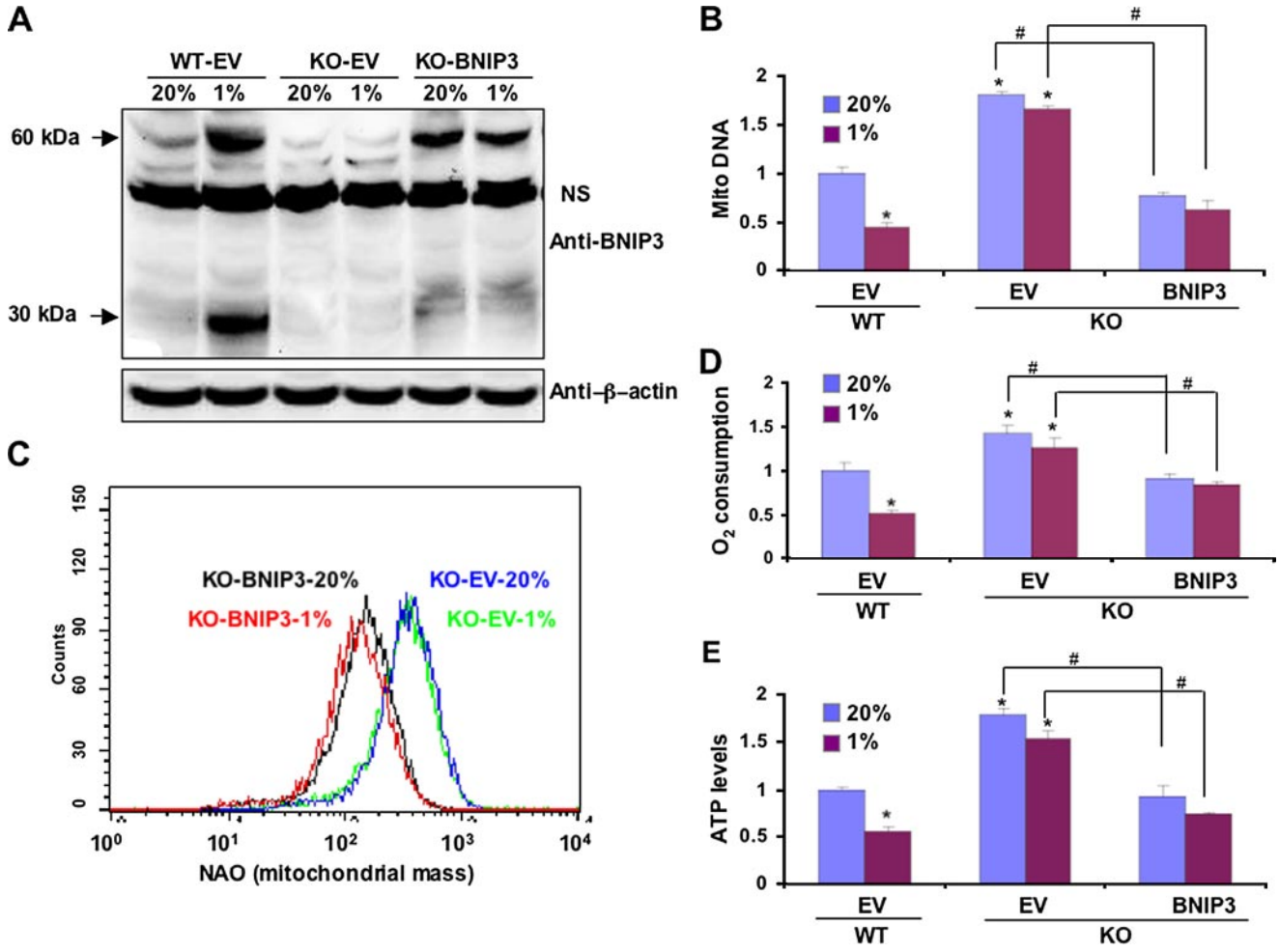

FIGURE 4. **Effect of BNIP3 gain-of-function on mitochondrial mass and respiration in WT and KO MEFs.** *A*, immunoblot analysis showed expression of BNIP3 protein in KO-BNIP3 MEFs cultured at 20 or 1% O_2 for 48 h. β-Actin served as a loading control. *NS*, nonspecific band. Mitochondrial DNA content (*B*), mitochondrial mass (*C*), O_2 consumption (*D*), and ATP levels (*E*) were measured in WT-EV, KO-EV, and KO-BNIP3 MEFs cultured at 20 or 1% O_2 for 48 h. Data are presented as the mean (±S.E.). *, $p < 0.05$ by Student's *t* test compared with WT-EV MEFs at 20% O_2; #, $p < 0.05$ for the indicated comparison (*bent lines*).

cells in a 0.4-ml volume were placed into the chamber of an Oxytherm unit (Hansatech Instrument Ltd.), which uses a Clark-type microelectrode to monitor the dissolved O_2 concentration in the sealed chamber over time. The data were exported to a computerized chart recorder (Oxygraph, Hansatech Instrument Ltd.), which calculated the rate of O_2 consumption. The temperature was maintained at 37 °C during the measurement. The rate of O_2 decline in 0.4 ml of Dulbecco's modified Eagle's medium without cells was measured to provide the background value. For each MEF subclone, the relative O_2 consumption rate was calculated by subtracting the background from the value obtained and dividing by the result obtained for WT MEFs at 20% O_2.

Intracellular ATP Measurement—ATP levels in MEFs were measured using an ATP assay kit (Sigma) according to the manufacturer's instructions. Luminescence was measured using a Wallac microplate luminescence reader (PerkinElmer Life Sciences) and normalized to the protein concentration.

Small Interfering RNA (siRNA) Experiments—siRNA targeting mouse Atg5 (siGENOME SMARTpool) and RISC-free control siRNA was purchased from Dharmacon Research Inc. Transfection of siRNA was performed with Oligofectamine reagent (Invitrogen) according to the manufacturer's instructions. After 24 h, cells were exposed to 20% or 1% O_2 for 48 h.

Measurement of Autophagosome Formation—cDNA encoding mouse LC3 was inserted into BglII- and KpnI-digested pEGFP-C1 (Clontech). Empty vector expressing green fluorescent protein (GFP) or vector expressing GFP-LC3 was transfected into MEFs grown on chamber slides. After overnight incubation, cells were exposed to 1% O_2 for 24 h and observed under a fluorescence microscope (Zeiss), and the percentage of cells with punctuate GFP-LC3 fluorescence was calculated.

Statistical Analysis—Data were expressed as the mean ± S.E. Statistical analysis was performed using Student's *t* test, and $p < 0.05$ was considered significant.

RESULTS

We previously demonstrated that in von Hippel-Lindau protein-deficient renal carcinoma cells, the constitutive activation of HIF-1 inhibits mitochondrial biogenesis by repressing c-Myc activity (25). In the present study we investigated whether HIF-1 regulates mitochondrial mass in an O_2-dependent manner in non-transformed MEFs and in normal mouse tissues *in vivo*. MEFs that were WT or homozygous for a knock-out allele

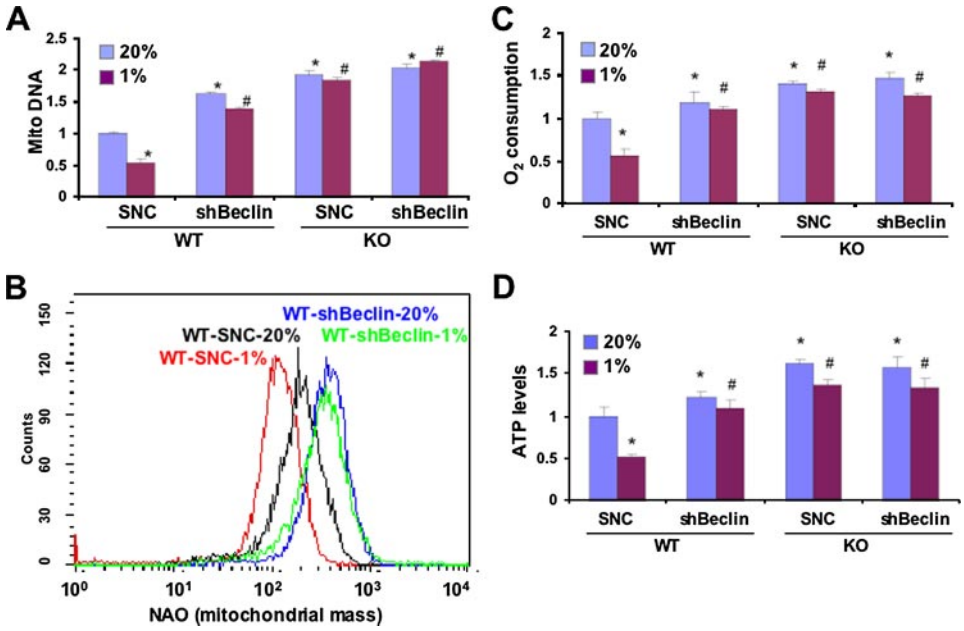

FIGURE 5. **Beclin-1 is required for HIF-1-dependent regulation of mitochondrial mass and respiration in MEFs.** Subclones of WT and KO MEFs expressing short hairpin RNA directed against Beclin-1 (*shBeclin*) or a scrambled negative control (*SNC*) were cultured at 20 or 1% O_2 for 48 h. Mitochondrial DNA content (*A*), mitochondrial mass (*B*), O_2 consumption (*C*), and ATP levels (*D*) were measured. Mean values are shown (±S.E.). *, $p < 0.05$ by Student's *t* test compared with WT-SNC at 20% O_2; #, $p < 0.05$ compared with WT-SNC at 1% O_2.

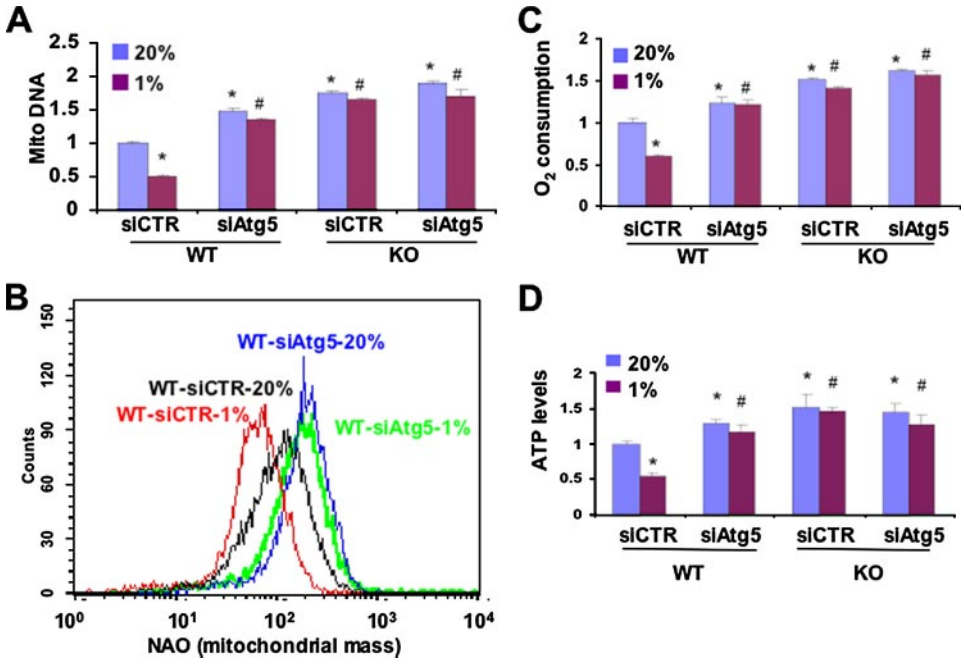

FIGURE 6. **Atg5 is required for HIF-1-dependent regulation of mitochondrial mass and respiration in MEFs.** WT and KO MEFs were transfected with siRNA directed against Atg5 (*siAtg5*) or a control siRNA (*siCTR*) and cultured at 20 or 1% O_2 for 48 h. Mitochondrial DNA content (*A*), mitochondrial mass (*B*), O_2 consumption (*C*), and ATP levels (*D*) were measured. Mean values are shown (±S.E.). *, $p < 0.05$ by Student's *t* test compared with WT-siCTR at 20% O_2; #, $p < 0.05$ compared with WT-siCTR at 1% O_2.

(KO) at the locus encoding HIF-1α (34) were cultured in complete medium in the presence of 20 or 1% O_2 for 48 h, and levels of mitochondrial DNA relative to nuclear DNA were determined by quantitative real-time PCR. Compared with WT MEFs, the levels of mitochondrial DNA were significantly increased in KO MEFs cultured at 20% O_2 (Fig. 1*A*). Exposure of WT cells to 1% O_2 resulted in a 4-fold decrease in mitochondrial DNA levels. In contrast, the mitochondrial DNA levels in KO cells cultured at 20 and 1% O_2 were not significantly different. Staining with NAO, a metachromatic dye that binds to cardiolipin in mitochondria regardless of their energetic state or membrane potential, revealed that mitochondrial mass was increased in KO as compared with WT MEFs at 20% O_2 and was further decreased in WT, but not KO, MEFs in response to hypoxia (Fig. 1*B*). O_2 consumption was significantly increased in KO as compared with WT MEFs cultured at 20% O_2, and hypoxia led to decreased O_2 consumption in WT, but not KO, MEFs (Fig. 1*C*). The increased O_2 consumption by KO MEFs was associated with increased intracellular ATP levels (Fig. 1*D*). The effects of hypoxia and HIF-1α deficiency on mitochondria were highly selective, as no changes in the mass of endoplasmic reticulum were detected by flow cytometry (Fig. 1*E*). Stable transfection with an expression vector encoding a constitutively active form of HIF-1α (15) was sufficient to significantly reduce mitochondrial DNA levels in KO MEFs (cultured at 20% O_2) as compared with KO MEFs transfected with empty vector (Fig. 1*F*). These studies demonstrate that prolonged exposure of MEFs to hypoxia results in a HIF-1-dependent reduction in mitochondrial mass and respiration.

To establish whether the tissue culture results were relevant to *in vivo* physiology, we analyzed lung tissue from normoxic littermate mice, which were WT or HET for the HIF-1α knock-out allele (22). Partial deficiency of HIF-1α was sufficient to increase mitochondrial DNA levels in the lungs of mice maintained in room air (Fig. 1*G*). Similar data were obtained by analysis of heart tissue from the same mice (supplemental Fig. S1). We also analyzed mice that were homozygous for a floxed allele at the HIF-1β locus and either carried a *Tie2-Cre* transgene (Cre^+), which inactivated both HIF-1β alleles (35) specifically in endothelial cells, or were non-transgenic (Cre^-) and continued to express HIF-1β.

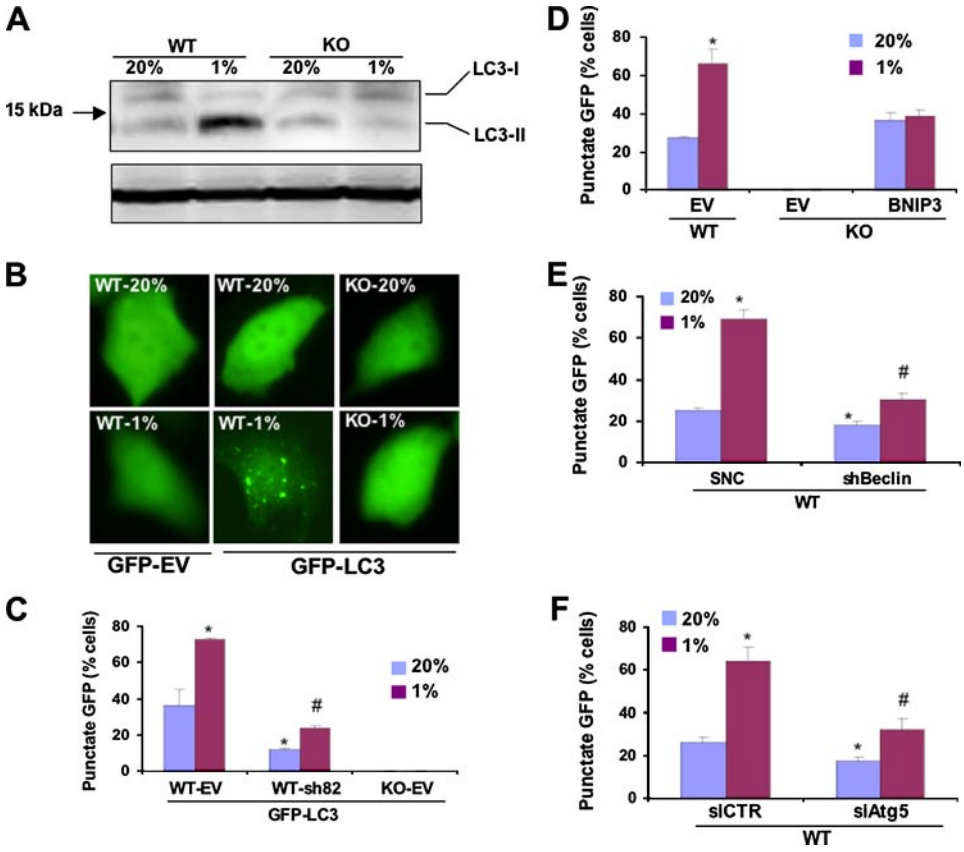

FIGURE 7. **HIF-1 activates BNIP3-, Beclin-1-, and Atg5-dependent autophagy in hypoxic MEFs.** *A*, WT and KO MEFs were incubated at 20 or 1% O_2 for 48 h, and whole cell lysates were subjected to immunoblot assay using an anti-LC3 antibody. *B*, WT and KO MEFs were transiently transfected with vector encoding GFP or GFP-LC3, incubated at 20% or 1% O_2, and analyzed by fluorescence microscopy. *C*, KO-EV MEFs and WT MEF subclones, which were stably transfected with EV or vector expressing short hairpin RNA directed against BNIP3 (sh82), were transiently transfected with vector GFP-LC3, cultured at 20 or 1% O_2, and analyzed by fluorescence microscopy. The percentage of cells exhibiting punctate fluorescence was calculated relative to all GFP-positive cells. Mean data (±S.E.) are shown. *, $p < 0.05$ compared with GFP-LC3-transfected WT-EV MEFs at 20% O_2; #, $p < 0.05$ compared with GFP-LC3-transfected WT-EV MEFs at 1% O_2. *D*, the percentage of cells with punctuate GFP-LC3 fluorescence was calculated relative to all fluorescent cells in WT-EV, KO-EV, and KO-BNIP3 MEF subclones. *, $p < 0.05$ compared with WT-EV at 20% O_2. *E*, the percentage of cells with punctuate GFP-LC3 fluorescence was calculated in WT MEF subclones expressing short hairpin RNA directed against Beclin1 (*shBeclin*) or a SNC. Mean data (±S.E.) are shown. *, $p < 0.05$ compared with WT-SNC at 20% O_2; #, $p < 0.05$ compared with WT-SNC at 1% O_2. *F*, the percentage of cells with punctuate GFP-LC3 fluorescence was calculated in WT MEF subclones expressing small interfering RNA against Atg5 (*siAtg5*) or a negative control siRNA (*siCTR*). Mean data (±S.E.) are shown. *, $p < 0.05$ compared with WT-siCTR at 20% O_2; #, $p < 0.05$ compared with WT-siCTR at 1% O_2.

Despite the fact that endothelial cells constitute no more than 50% of all cells in the lung, a significant increase in mitochondrial DNA levels was observed in the Cre^+ mice compared with their Cre^- littermates (Fig. 1*H*). These studies demonstrate that HIF-1 regulates mitochondrial mass under normal physiological conditions *in vivo*.

BNIP3 is a known HIF-1 target gene (36–38) that has been implicated in autophagy (33). Recent studies indicate that BH3-only proteins such as BNIP3 may induce autophagy by disrupting interactions between Beclin-1, a highly conserved protein that is required for the initiation of autophagy, and Bcl2 or Bcl-X_L (39). Exposure of WT MEFs to 1% O_2 for 24 h dramatically induced the expression of BNIP3 mRNA as determined by quantitative real-time RT-PCR (Fig. 2*A*). Very low levels of BNIP3 protein were detected by immunoblot assay of lysates prepared from WT MEFs that were cultured at 20% O_2 (Fig. 2*B*), whereas hypoxia strongly induced expression of BNIP3 protein, which migrated as a 30-kDa monomer and 60-kDa dimer, as previously described (37). Little or no BNIP3 mRNA and protein was detectable in KO MEFs cultured at 20 or 1% O_2. The expression of BNIP3 mRNA and protein was significantly reduced in the lungs of HET (as compared with WT; Figs. 2, *C* and *D*) and Cre^+ (as compared with Cre^-; Figs. 2, *E* and *F*) mice, demonstrating that BNIP3 expression is regulated by HIF-1 under physiological conditions *in vivo*.

Based on the results presented in Figs. 1 and 2, we hypothesized that HIF-1-dependent BNIP3 expression influences mitochondrial mass under physiological conditions by determining the rate of mitochondrial autophagy. However, HIF-1 loss-of-function studies are not sufficient to address this issue, because HIF-1 has been shown to regulate mitochondrial biogenesis (25), and thus, the observed reduction in mitochondria may result from decreased production rather than increased destruction of mitochondria. Because BNIP3 is involved in autophagy but not mitochondrial biogenesis, we analyzed the effect of knocking down BNIP3 expression by RNA interference using two different short hairpin RNAs, designated sh80 and sh82, which reduced BNIP3 mRNA (Fig. 3*A*) and protein (Fig. 3*B*) in WT MEFs to levels intermediate between those of WT and KO MEFs. Compared with WT MEFs stably transfected with empty vector, mitochondrial DNA levels (Fig. 3*C*) and mitochondrial mass (Fig. 3*D*) were significantly increased in WT MEFs transfected with expression vector encoding sh80 or sh82. As in the case of HIF-1α-deficient KO MEFs (Fig. 1*B*), hypoxia did not induce a decrease in mitochondrial DNA levels or mitochondrial mass in WT MEFs with short hairpin RNA-mediated BNIP3 knockdown (Figs. 3, *C* and *D*). O_2 consumption (Fig. 3*E*) and ATP levels (Fig. 3*F*) were increased in WT MEFs expressing sh80 or sh82, both at 20 and 1% O_2. These data demonstrate that the reduction in mitochondrial DNA, mitochondrial mass, and cell respiration in response to hypoxia are dependent upon the expression of BNIP3.

We next analyzed the effect of stably transfecting KO MEFs with an expression vector encoding BNIP3. The resulting KO-BNIP3 subclone constitutively expressed BNIP3 protein at levels slightly less than those observed in WT MEFs cultured under hypoxic conditions (Fig. 4*A*). Compared with KO MEFs

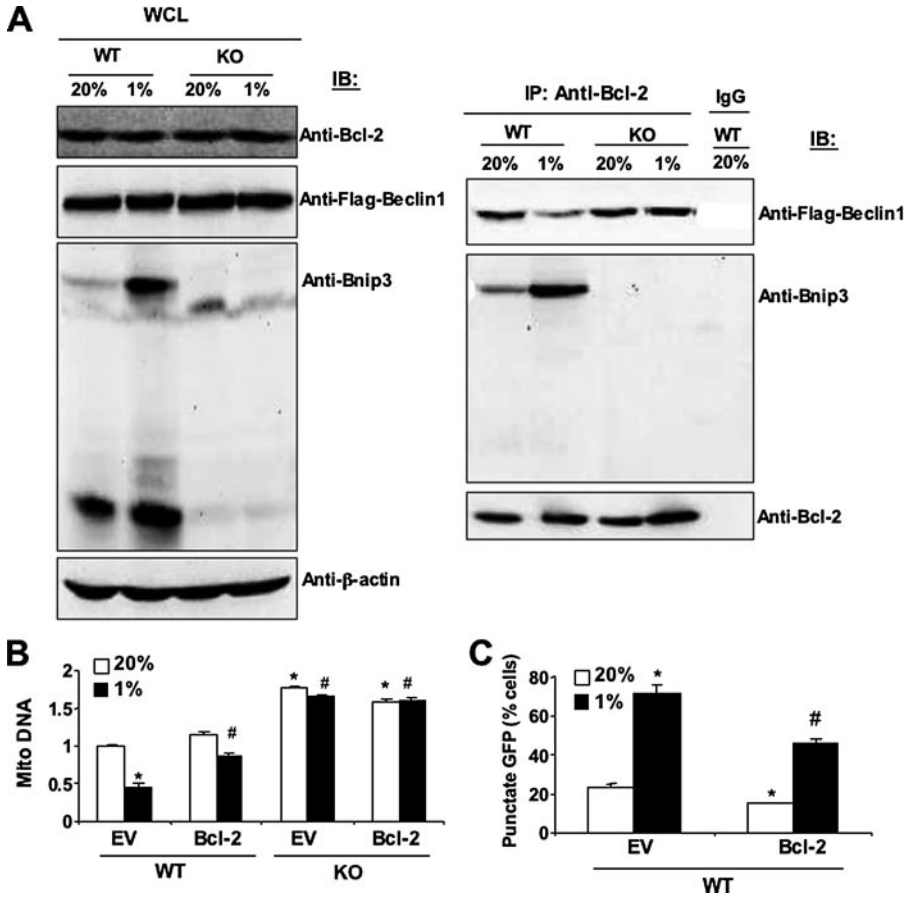

FIGURE 8. **BNIP3 competes with Beclin-1 for binding to Bcl2.** *A*, MEFs were exposed to 20 or 1% O_2 for 48 h, whole cell lysates (*WCL*) were prepared, and aliquots were subjected to direct immunoblot assays (*IB*, *left panel*) or after immunoprecipitation (*IP*) with anti-Bcl2 antibody (*right panel*). *B* and *C*, MEFs stably transfected with EV or vector encoding Bcl2 were exposed to 20 or 1% O_2 for 48 h and analyzed for mitochondrial:nuclear DNA ratio (*B*) or punctate fluorescence of GFP-LC3 (*C*). Mean data (±S.E.) are shown. *, $p < 0.05$ compared with WT-EV at 20% O_2; #, $p < 0.05$ compared with WT-EV at 1% O_2.

stably transfected with empty vector (KO-EV), mitochondrial DNA levels (Fig. 4*B*) and mitochondrial mass (Fig. 4*C*) were constitutively reduced in KO-BNIP3 MEFs. O_2 consumption (Fig. 4*D*) and ATP levels (Fig. 4*E*) were also significantly decreased in KO-BNIP3 as compared with KO-EV MEFs. Thus, BNIP3 expression is sufficient to reduce mitochondrial mass and respiration.

If the observed differences in mitochondrial mass and metabolism between WT and KO MEFs were due to mitochondrial autophagy in WT cells that was lost in KO cells, then interference with expression of Beclin-1, a key regulator of autophagy, should eliminate these differences by eliminating autophagy in WT MEFs. Expression of Beclin-1 mRNA was not significantly different in parental (untransfected) WT and KO MEFs (supplemental Fig. S2). Beclin-1 mRNA levels were similarly reduced in WT and KO MEFs stably transfected with a vector encoding a short hairpin RNA targeting Beclin-1 (shBeclin) but were not significantly changed in WT and KO MEFs transfected with a vector encoding a scrambled negative control short hairpin RNA (SNC). Knockdown of Beclin-1 had no effect on the levels of BNIP3 mRNA (supplemental Fig. S3) or protein (supplemental Fig. S4). WT-shBeclin MEFs were similar to WT-sh82 and KO MEFs in manifesting increased mitochondrial DNA levels (Fig. 5*A*) and mitochondrial mass (Fig. 5*B*), which did not decrease in response to hypoxia, as well as increased O_2 consumption (Fig. 5*C*) and ATP levels (Fig. 5*D*). Identical results were obtained using small interfering siRNA against Atg5, another key component of the autophagy machinery (Fig. 6). The requirement for Beclin-1 and Atg5 provides strong evidence that autophagy plays a critical role in the reduction in mitochondrial mass and respiration that is induced when WT MEFs are exposed to hypoxia.

To confirm the involvement of autophagy by additional independent assays, we analyzed LC3-I to LC3-II protein processing, which is a hallmark of autophagy. Levels of endogenous LC3-II were markedly increased in WT cells incubated at 1% O_2 as compared with 20% O_2 or compared with KO cells at 20 or 1% O_2 (Fig. 7*A*). As another independent assay of autophagy, MEFs were transiently transfected with an expression vector encoding GFP or a GFP-LC3 fusion protein, which is concentrated in autophagic vacuoles, resulting in punctate fluorescence within cells undergoing autophagy. GFP was expressed homogeneously throughout WT MEFs regardless of the O_2 concentration (Fig. 7*B*). In contrast, a proportion of WT MEFs expressing GFP-LC3 manifested punctate fluorescence when cultured at 20% O_2, and the percentage of such cells increased significantly in response to hypoxia (Fig. 7, *B* and *C*). Compared with WT-EV MEFs, the percentage of WT-sh82 cells (with BNIP3 knockdown) that manifested punctate fluorescence was significantly decreased at both 20 and 1% O_2 (Fig. 7*C*). Remarkably, KO-EV cells, which lack BNIP3 expression, showed no punctate fluorescence of GFP-LC3 regardless of the O_2 concentration.

Forced expression of BNIP3 in KO MEFs resulted in the appearance of cells with punctate fluorescence, but the percentage of such cells did not increase in response to hypoxia (Fig. 7*D*). Compared with WT-SNC MEFs, WT-shBeclin cells (with Beclin1 knockdown) manifested significantly decreased punctate fluorescence, especially at 1% O_2 (Fig. 7*E*). Similar results were observed for WT MEFs transfected with siRNA against Atg5 (Fig. 7*F*). The striking concordance of the LC3 data in Fig. 7 with the data presented in Figs. 1–6 establish that autophagy plays a key role in the reduced mitochondrial mass and respiration observed in hypoxic WT MEFs and that hypoxia-induced autophagy is dependent upon the constitutive

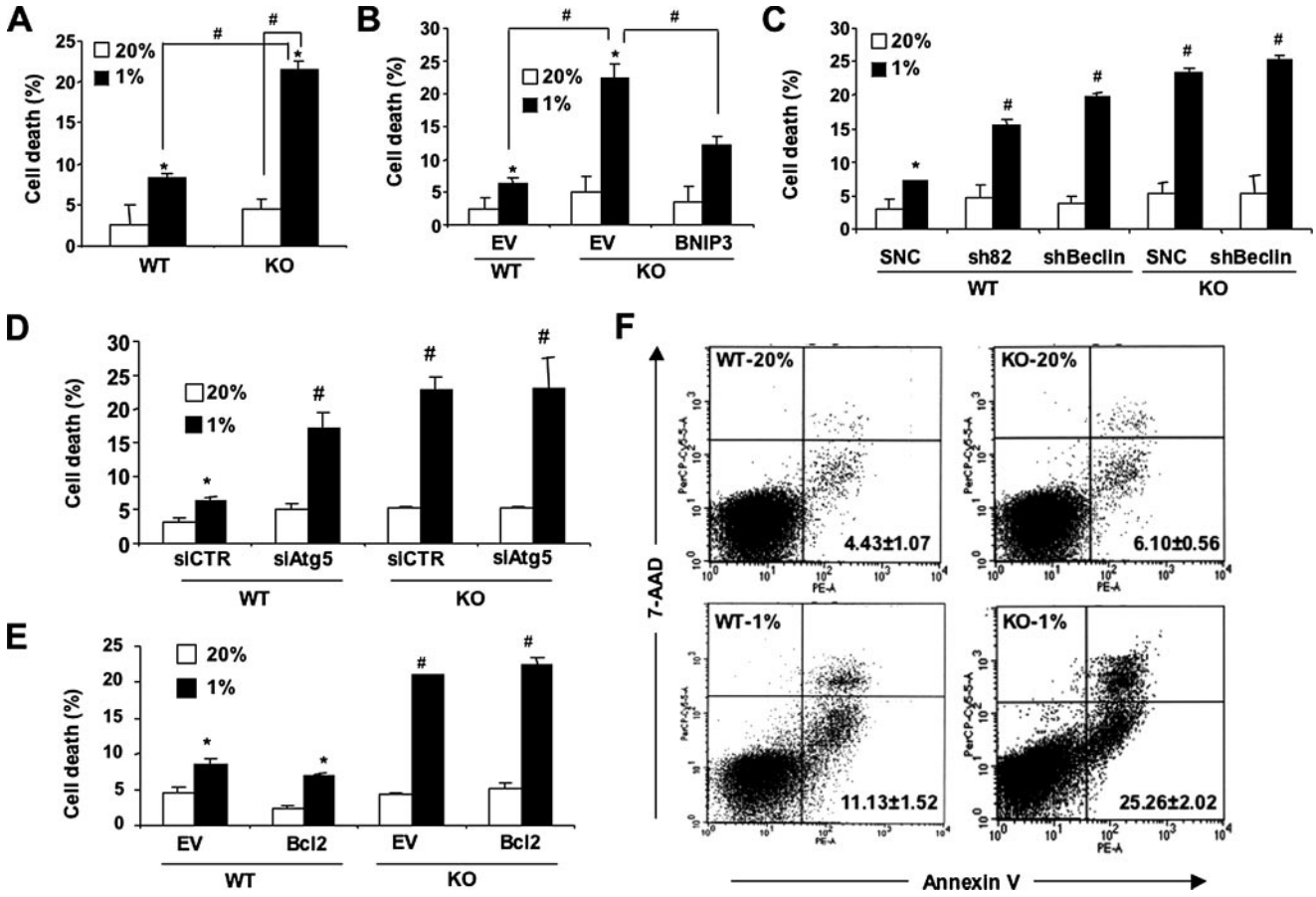

FIGURE 9. **Protective effect of HIF-1/BNIP3/Beclin/Atg6-induced autophagy in hypoxic cells.** *A*, *B*, *C*, *D*, and *E*, the indicated MEF subclones were cultured at 20 or 1% O_2 for 48 h, and the number of dead cells as a percentage of total cell number was determined by trypan blue staining. Mean data (±S.E.) are shown. *, $p < 0.05$ by Student's *t* test compared with the control WT MEF subclone in the first column of each bar graph. #, $p < 0.05$ for indicated comparison (*A* and *B*) or compared with WT-SNC (*C*), siCTR (*D*), or WT-EV (*E*) at 1% O_2. *F*, MEFs were cultured at 20 or 1% O_2 for 48 h and then incubated with 7-AAD and phosphatidylethanolamine-labeled anti-annexin V antibody for flow cytometric analysis of apoptosis. The percentage (mean ± S.E.) of annexin$^+$/7-AAD$^-$ cells are shown.

expression of Beclin-1 and Atg5 as well as the HIF-1-mediated induction of BNIP3 expression.

Recent studies indicate that BH3-only proteins such as BNIP3 may play an important role in the induction of autophagy by disrupting the interaction of Beclin-1, which also contains a BH3 domain, with Bcl2 or Bcl-X_L (39, 40). Immunoblot analysis of MEF lysates for Bcl2 and Beclin-1 revealed that each protein was present at equal levels in WT and KO cells regardless of O_2 concentration (Fig. 8*A*, *left panel*). Immunoprecipitation of the lysates with anti-Bcl2 antibodies revealed increased interaction of BNIP3 with Bcl2 in WT cells under hypoxic as compared with non-hypoxic conditions (Fig. 8*A*, *right panel*) as expected based on the increased levels of BNIP3 protein (Fig. 8*A*, *left panel*). The increased interaction of Bcl2 with BNIP3 was accompanied by decreased interaction of Bcl2 with Beclin-1 in hypoxic WT cells (Fig. 8*A*, *right panel*). In contrast, the interaction of Bcl2 with Beclin-1 was not affected by O_2 concentration in KO cells, in which BNIP3 was not induced by hypoxia. Overexpression of Bcl2 (supplemental Fig. S5) increased mitochondrial DNA levels (Fig. 8*B*) and inhibited autophagy (Fig. 8*C*) in WT MEFs, especially under hypoxic conditions. Exposure of Bcl2-overexpressing cells to hypoxia resulted in increased BNIP3 interaction and decreased Beclin-1 interaction with Bcl2 in WT, but not in KO, MEFs as determined by co-immunoprecipitation assays (supplemental Fig. S6). These results support the conclusion that hypoxia-induced BNIP3 competes with Beclin-1 for binding to Bcl2 and thereby increases the levels of free Beclin-1, which trigger autophagy.

The functional significance of autophagy has been poorly understood, primarily because many of the studies have not been performed in an appropriate physiological context. We hypothesized that hypoxia-induced mitochondrial autophagy promoted cell survival under hypoxic conditions. Hypoxia-induced cell death was significantly increased in KO as compared with WT MEFs (Fig. 9*A*). In contrast, BNIP3 overexpression reduced hypoxia-induced KO cell death (Fig. 9*B*). Beclin-1 or BNIP3 (Fig. 9*C*) or Atg5 (Fig. 9*D*) knockdown increased hypoxia-induced cell death in WT MEFs. In contrast to BNIP3, overexpression of Bcl2 did not prevent hypoxia-induced cell death in KO MEFs (Fig. 9*E*). Analysis of Annexin V$^+$/7-AAD$^-$ cells by flow cytometry demonstrated that apoptosis, which was more severe in KO than in WT MEFs, contributed to hypoxia-induced cell death (Fig. 9*F*).

To investigate the role of ROS in hypoxia-induced cell death, MEFs were incubated with the non-fluorescent compound dichlorodihydrofluorescein diacetate, which in the

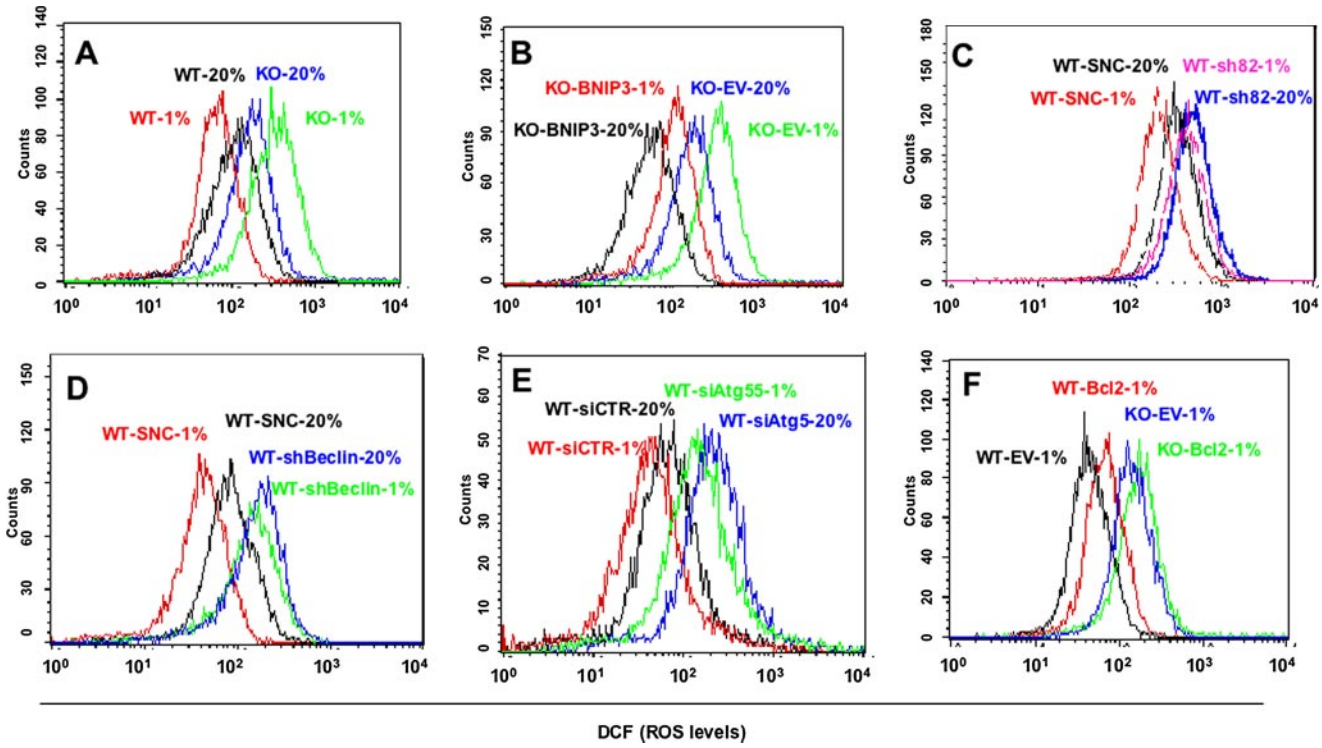

FIGURE 10. **Analysis of ROS levels.** Equal numbers of the indicated MEF subclones were cultured at 20 or 1% O_2 for 48 h and stained with 1 μM dichlorodihydrofluorescein diacetate, and oxidative metabolism to dichlorofluorescein (*DCF*) was determined by flow cytometry.

presence of ROS is oxidized to the highly fluorescent dichlorofluorescein. Flow cytometry was performed to quantify the dichlorofluorescein signal. Exposure of KO MEFs to 1% O_2 for 48 h resulted in a marked increase in ROS levels, in contrast to WT MEFs, in which ROS levels decreased in response to hypoxia (Fig. 10*A*). Forced expression of BNIP3 in KO MEFs reduced ROS levels (Fig. 10*B*). Although ROS levels were decreased in KO-BNIP3 compared with KO-EV MEFs, prolonged hypoxia resulted in increased ROS levels in BNIP3-KO MEFs, whereas in WT MEFs, ROS levels decreased under conditions of chronic hypoxia. These findings are consistent with the absence in BNIP3-KO MEFs of other adaptive responses to hypoxia that occur in WT cells, such as COX4 subunit switching (19) and PDK1 expression (20). Loss of function for BNIP3 (Fig. 10*C*), Beclin-1 (Fig. 10*D*), or Atg5 (Fig. 10*E*) was associated with increased ROS levels, as was increased Bcl2 expression (Fig. 10*F*).

To determine whether increased ROS levels contributed to cell death, MEFs were subjected to hypoxia in the presence or absence of the free radical scavenger MnTMPyP. Treatment with MnTMPyP had no effect on WT MEFs but markedly reduced ROS levels (Fig. 11*A*) and cell death (Fig. 11*B*) in hypoxic KO MEFs.

DISCUSSION

Our recent studies have demonstrated that HIF-1 plays an essential role by maintaining an optimal balance between the competing demands of energy and redox homeostasis over the physiological range of O_2 concentrations (19, 20, 25). Whereas consideration of cellular energetics favors oxidative metabolism as the most efficient means of producing adequate levels of ATP to maintain cell survival, mitochondrial respiration is also associated with increased ROS generation, which if unchecked can cause cell death.

Acute exposure of cells to hypoxia results in an acute increase in ROS generation by complex III of the mitochondrial electron transport chain (9, 10). Reduced O_2 availability and increased ROS levels inhibit the activity of the prolyl hydroxylases that target HIF-1α for ubiquitination and proteasomal degradation (5–7, 10). We have identified three HIF-1-dependent molecular mechanisms by which cells adapt their energy metabolism to hypoxic conditions: COX4 subunit switching (19), inhibition of acetyl-CoA synthesis by activation of *PDK1* (20), and inhibition of mitochondrial biogenesis by repression of c-Myc activity (25). In each of these studies failure to properly regulate mitochondrial metabolism in response to hypoxia was associated with increased ROS levels and increased cell death.

The present study demonstrates that mitochondrial autophagy is a fourth component of the HIF-1-mediated metabolic adaptation that is required to prevent increased ROS levels and cell death in hypoxic MEFs. Our studies have demonstrated that WT MEFs exposed to 20% O_2 consume only half as much O_2 as KO MEFs. The reduction of the ambient O_2 concentration from 20 to 1% does not significantly impair O_2 consumption and ATP production by KO MEFs (Fig. 1, *C* and *D*) or MEFs with knockdown of BNIP3 (Fig. 3, *E* and *F*), Beclin-1 (Fig. 5, *C* and *D*), or Atg5 (Fig. 6, *C* and *D*). In striking contrast to conventional wisdom, we conclude that O_2 consumption is not passively reduced in hypoxic WT MEFs because of substrate limitation but instead is actively reduced because under hypoxic conditions the utilization of O_2 for respiration is inef-

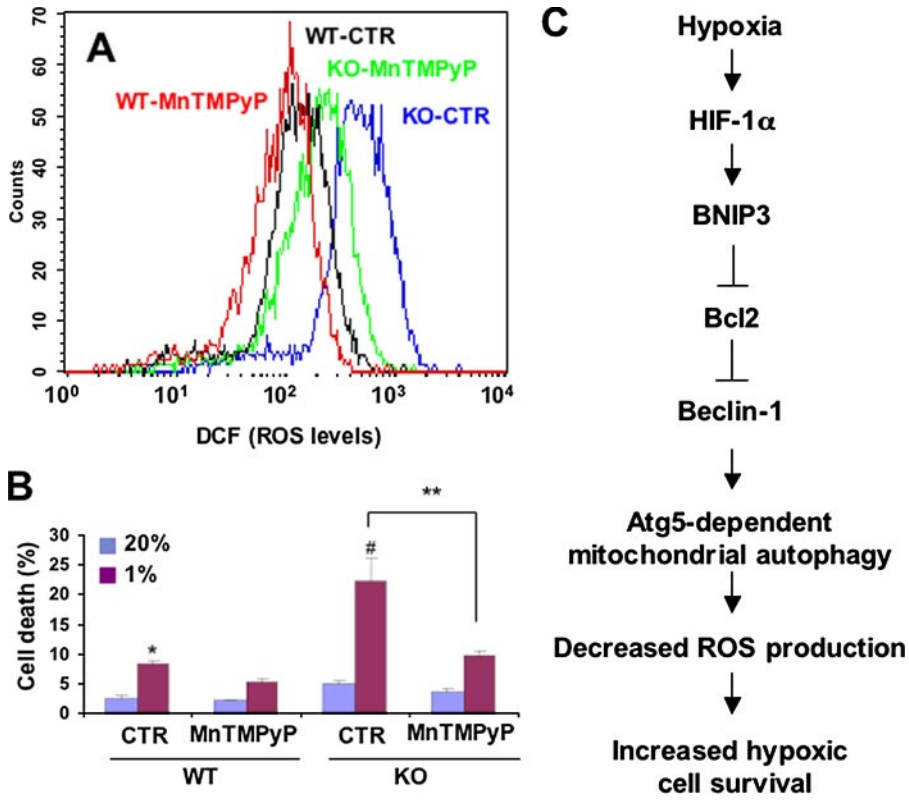

FIGURE 11. **ROS scavenger rescues HIF-1α-deficient MEFs from hypoxia-induced cell death.** MEFs were exposed to 20 or 1% O_2 for 48 h in the presence of 25 μM MnTMPyP, a superoxide dismutase mimetic, or vehicle control (*CTR*). *A*, ROS levels were quantified by dichlorofluorescein (*DCF*) fluorescence. *B*, percent cell death (mean ± S.E.) was quantified by trypan blue staining. *, $p < 0.05$ by Student's *t* test compared with WT-CTR at 20% O_2; #, $p < 0.05$ compared with WT-CTR at 1% O_2; **, $p < 0.05$ for indicated comparison. *C*, molecular pathway regulating mitochondrial autophagy, cell respiration, ROS levels, and cell survival in MEFs subjected to prolonged hypoxia.

ficient and, if unchecked, as in KO, WT-sh82, WT-shBeclin, or WT-siAtg5 MEFs, will lead to elevated levels of ROS and cell death. Thus, mitochondrial autophagy through BNIP3 activation-like COX4 subunit switching, PDK1 induction, and c-Myc repression represents a HIF-1-mediated adaptive response that enables cells to survive prolonged hypoxia (Fig. 11*C*).

Consistent with recent reports (39–41), our studies indicate that hypoxia selectively induces autophagy of mitochondria but not endoplasmic reticulum and that HIF-1-mediated expression of BNIP3 plays an important role in the induction of hypoxia-induced mitochondrial autophagy by disrupting the interaction of Beclin-1 with Bcl2. Although Beclin-1 was clearly required for hypoxia-induced autophagy in MEFs, there was no evidence for regulation of Beclin-1 by HIF-1, in contrast to a recent report that silencing of HIF-1 in cultured chondrocytes was associated with reduced Beclin-1 levels (42). The demonstration that loss of function of a key component of the autophagy machinery (Beclin-1 or Atg5) phenocopies the loss of hypoxic adaptation that is associated with HIF-1α or BNIP3 loss of function provides compelling evidence for the role of autophagy in MEF survival under conditions of prolonged hypoxia.

It should be noted that studies of GFP-LC3 fluorescence suggested ongoing autophagy in WT MEFs at 20% O_2. BNIP3 was not expressed in WT MEFs at 20% O_2, suggesting that another BH3-only protein may be responsible. Because GFP-LC3 analysis showed no evidence of autophagy in KO MEFs, expression of the protein responsible for autophagy at 20% O_2 must also be HIF-1-dependent. Among the other known BH3-domain-only proteins, HIF-1 has been shown to regulate the expression of BNIP3L/NIX (37, 15), HGTD-P (43), and NOXA (44). Studies of these proteins in cancer cells had previously linked them to hypoxia-induced cell death. Thus, further studies are required to investigate the potential role of these proteins in HIF-1-dependent autophagy.

While this manuscript was in preparation, the retinoblastoma protein was reported to antagonize HIF-1-mediated transactivation of the *Bnip3* promoter (45). BNIP3 was required for autophagy induced by serum and O_2 deprivation or by treatment with iron chelators or other inhibitors of prolyl hydroxylases. However, the role of HIF-1 in this process was not investigated, and autophagy was viewed as an intermediate step in the process of non-apoptotic cell death. In contrast, our data indicate that autophagy is an adaptive response, with cell death representing the outcome of failed adaptation.

In the present study we have provided experimental evidence supporting the conclusion that HIF-1-mediated alterations in mitochondrial metabolism are critical to understanding the mechanisms and consequences of hypoxia-induced autophagy. Our analyses of MEFs demonstrate that mitochondrial autophagy is an adaptive metabolic response that promotes the survival of cells under conditions of prolonged hypoxia (Fig. 11*C*). This process requires the HIF-1-dependent induction of BNIP3 and the autophagy machinery as demonstrated by Beclin-1 and Atg5 loss-of-function studies and the assessment of GFP-LC3 protein subcellular localization. Furthermore, we demonstrate that HIF-1 regulates mitochondrial mass under normal physiological conditions, as even partial deficiency of HIF-1α had a profound effect on BNIP3 expression and mitochondrial mass in the lungs of mice exposed to room air.

These results are consistent with the view of mitochondrial autophagy as an important component of the toolkit utilized by HIF-1 to maintain O_2 homeostasis. Taken together with other recent studies (19, 20, 25), these data reinforce the conclusion that O_2, energy, and redox homeostasis are inextricably linked and that the maintenance of an optimal balance between their competing interests is essential to cell survival. Understanding the factors that determine which of these adaptive metabolic responses to hypoxia are utilized by any given cell *in vivo* and

whether these adaptations are successful in preventing cell death remains a formidable challenge for future studies.

Acknowledgments—We thank L. Cheng and R. Siliciano for providing the Bcl2 lentiviral vector and C. Dang for use of the Oxytherm oxygen electrode.

REFERENCES

1. Lehninger, A. L. (1975) *Biochemistry*, Worth Publishers, Inc., New York
2. Melillo, G. (2004) *Cell Cycle* **3,** 154–155
3. Brahimi-Horn, M. C., and Pouyssegur, J. (2007) *FEBS Lett.* **581,** 3582–3591
4. Wang, G. L., Jiang, B. H., Rue, E. A., and Semenza, G. L. (1995) *Proc. Natl. Acad. Sci. U. S. A.* **92,** 5510–5514
5. Dann, C. E., III, and Bruick, R. K. (2005) *Biochem. Biophys. Res. Commun.* **338,** 639–647
6. Kaelin, W. G., Jr. (2005) *Biochem. Biophys. Res. Commun.* **338,** 627–638
7. Schofield, C. J., and Ratcliffe, P. J. (2005) *Biochem. Biophys. Res. Commun.* **338,** 617–626
8. Pan, Y., Mansfield, K. D., Bertozzi, C. C., Rudenko, V., Chan, D. A., Giaccia, A. J., and Simon, M. C. (2007) *Mol. Cell. Biol.* **27,** 912–925
9. Chandel, N. S., McClintock, D. S., Feliciano, C. E., Wood, T. M., Melendez, J. A., Rodriguez, A. M., and Schumacker, P. T. (2000) *J. Biol. Chem.* **275,** 25130–25138
10. Guzy, R. D., Hoyos, B., Robin, E., Chen, H., Liu, L., Mansfield, K. D., Simon, M. C., Hammerling, U., and Schumacker, P. T. (2005) *Cell Metab.* **1,** 401–408
11. Salceda, S., and Caro, J. (1997) *J. Biol. Chem.* **272,** 22642–22647
12. Kallio, P. J., Wilson, W. J., O'Brien, S., Makino, Y., and Poellinger, L. (1999) *J. Biol. Chem.* **274,** 6519–6525
13. Maxwell, P. H., Wiesener, M. S., Chang, G. W., Clifford, S. C., Vaux, E. C., Cockman, M. E., Wykoff, C. C., Pugh, C. W., Maher, E. R., and Ratcliffe, P. J. (1999) *Nature* **399,** 271–275
14. Kamura, T., Sato, S., Iwai, K., Czyzyk-Krzeska, M., Conaway, R. C., and Conaway, J. W. (2000) *Proc. Natl. Acad. Sci. U. S. A.* **97,** 10430–10435
15. Manalo, D. J., Rowan, A., Lavoie, T., Natarajan, L., Kelly, B. D., Ye, S. Q., Garcia, J. G., and Semenza, G. L. (2005) *Blood* **105,** 659–669
16. Elvidge, G. P., Glenny, L., Appelhoff, R. J., Ratcliffe, P. J., Ragoussis, J., and Gleadle, J. M. (2006) *J. Biol. Chem.* **281,** 15215–15226
17. Semenza, G. L., and Wang, G. L. (1992) *Mol. Cell. Biol.* **12,** 5447–5454
18. Forsythe, J. A., Jiang, B. H., Iyer, N. V., Agani, F., Leung, S. W., Koos, R. D., and Semenza, G. L. (1996) *Mol. Cell. Biol.* **16,** 4604–4613
19. Fukuda, R., Zhang, H., Kim, J. W., Shimoda, L., Dang, C. V., and Semenza, G. L. (2007) *Cell* **129,** 111–122
20. Kim, J. W., Tchernyshyov, I., Semenza, G. L., and Dang, C. V. (2006) *Cell Metab.* **3,** 177–185
21. Papandreou, I., Cairns, R. A., Fontana, L., Lim, A. L., and Denko, N. C. (2006) *Cell Metab.* **3,** 187–197
22. Iyer, N. V., Kotch, L. E., Agani, F., Leung, S. W., Laughner, E., Wenger, R. H., Gassmann, M., Gearhart, J. D., Lawler, A. M., Yu, A. Y., and Semenza, G. L. (1998) *Genes Dev.* **12,** 149–162
23. Seagroves, T. N., Ryan, H. E., Lu, H., Wouters, B. G., Knapp, M., Thibault, P., Laderoute, K., and Johnson, R. S. (2001) *Mol. Cell. Biol.* **21,** 3436–3444
24. Lum, J. J., Bui, T., Gruber, M., Gordan, J. D., DeBerardinis, R. J., Covello, K. L., Simon, M. C., and Thompson, C. B. (2007) *Genes Dev.* **21,** 1037–1049
25. Zhang, H., Gao, P., Fukuda, R., Kumar, G., Krishnamachary, B., Zeller, K. I., Dang, C. V., and Semenza, G. L. (2007) *Cancer Cell* **11,** 407–420
26. Menzies, R. A., and Gold, P. H. (1971) *J. Biol. Chem.* **246,** 2425–2429
27. Levine, B., and Klionsky, D. J. (2004) *Dev. Cell* **6,** 463–477
28. Kundu, M., and Thompson, C. B. (2005) *Cell Death Differ.* **12,** 1484–1489
29. De Duve, C., and Wattiaux, R. (1966) *Annu. Rev. Physiol.* **28,** 435–492
30. Zhu, H., Tannous, P., Johnstone, J. L., Kong, Y., Shelton, J. M., Richardson, J. A., Le, V., Levine, B., Rothermel, B. A., and Hill, J. A. (2007) *J. Clin. Investig.* **117,** 1782–1793
31. Decker, R. S., and Wildenthal, K. (1980) *Am. J. Pathol.* **98,** 425–444
32. Yan, L., Vatner, D. E., Kim, S. J., Ge, H., Masurekar, M., Massover, W. H., Yang, G., Matsui, Y., Sadoshima, J., and Vatner, S. F. (2005) *Proc. Natl. Acad. Sci. U. S. A.* **102,** 13807–13812
33. Hamacher-Brady, A., Brady, N. R., Logue, S. E., Sayen, M. R., Jinno, M., Kirshenbaum, L. A, Gottlieb, R. A., and Gustafsson, A. B. (2007) *Cell Death Differ.* **14,** 146–157
34. Feldser, D., Agani, F., Iyer, N. V., Pak, B., Ferreira, G., and Semenza, G. L. (1999) *Cancer Res.* **59,** 3915–3918
35. Yim, S. H., Shah, Y., Tomita, S., Morris, H. D., Gavrilova, O., Lambert, G., Ward, J. M., and Gonzalez, F. J. (2006) *Hepatology* **44,** 550–560
36. Bruick, R. K. (2000) *Proc. Natl. Acad. Sci. U. S. A.* **97,** 9082–9087
37. Sowter, H. M., Ratcliffe, P. J., Watson, P., Greenberg, A. H., and Harris, A. L. (2001) *Cancer Res.* **61,** 6669–6673
38. Greijer, A. E., van der Groep, P., Kemming, D., Shvarts, A., Semenza, G. L., Meijer, G. A., van de Wiel, M. A., Belien, J. A., van Diest, P. J., and van der Wall, E. (2005) *J. Pathol.* **206,** 291–304
39. Maiuri, M. C., Le Toumelin, G., Criollo, A., Rain, J. C., Gautier, F., Juin, P., Tasdemir, E., Pierron, G., Troulinaki, K., Tavernarakis, N., Hickman, J. A., Geneste, O., and Kroemer, G. (2007) *EMBO J.* **26,** 2527–2539
40. Oberstein, A., Jeffrey, P. D., and Shi, Y. (2007) *J. Biol. Chem.* **282,** 13123–13132
41. Maiuri, M. C., Criollo, A., Tasdemir, E., Vicencio, J. M., Tajeddine, N., Hickman, J. A., Geneste, O., and Kroemer, G. (2007) *Autophagy* **3,** 374–376
42. Bohensky, J., Shapiro, I. M., Leshinsky, S., Terkhorn, S. P., Adams, C. S., and Srinivas, V. (2007) *Autophagy* **3,** 207–214
43. Lee, M. J., Kim, J. Y., Suk, K., and Park, J. H. (2004) *Mol. Cell. Biol.* **24,** 3918–3927
44. Kim, J. Y., Ahn, H. J., Ryu, J. H., Suk, K., and Park, J. H. (2004) *J. Exp. Med.* **199,** 113–124
45. Tracy, K., Dibling, B. C., Spike, B. T., Knabb, J. R., Schumacker, P., and Macleod, K. F. (2007) *Mol. Cell. Biol.* **27,** 6229–6242

Supplemental Data

S1

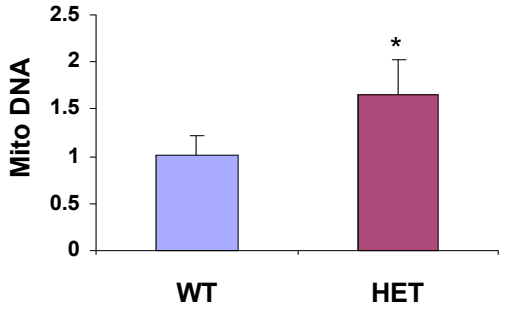

S2

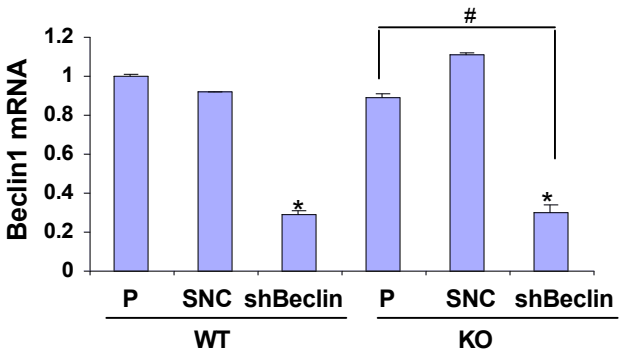

S3

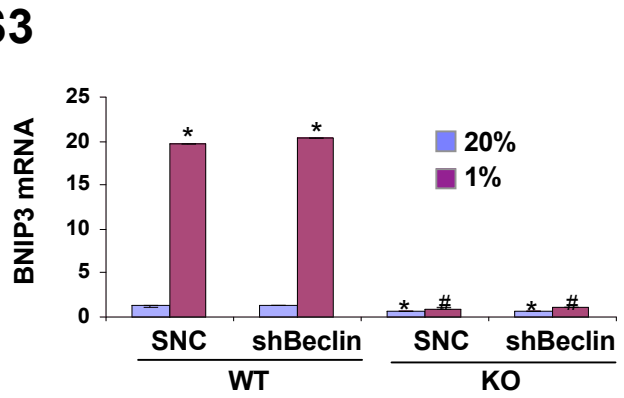

S4

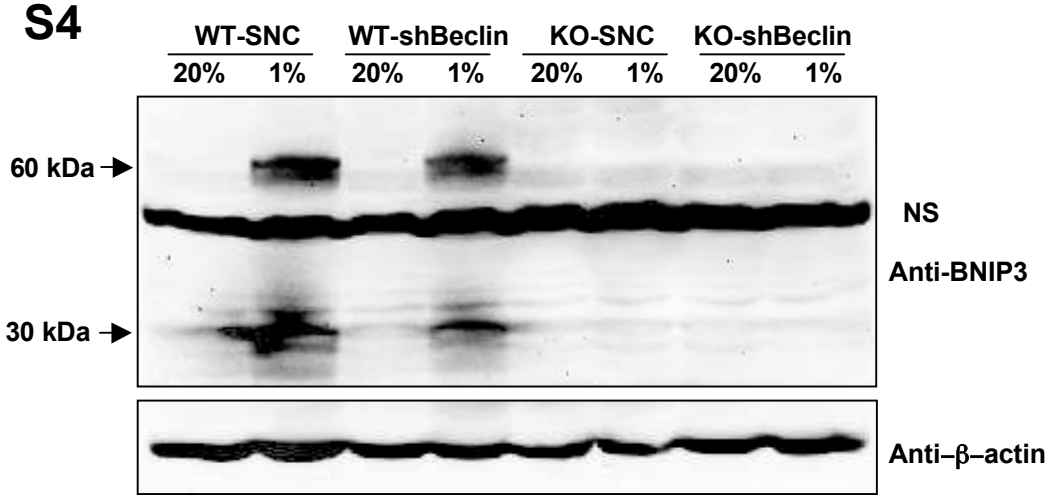
WT-SNC
WT-shBeclin
KO-SNC
KO-shBeclin
20%
1%
20%
1%
20%
1%
20%
1%
60 kDa
30 kDa
NS
Anti-BNIP3
Anti–β–actin

S5

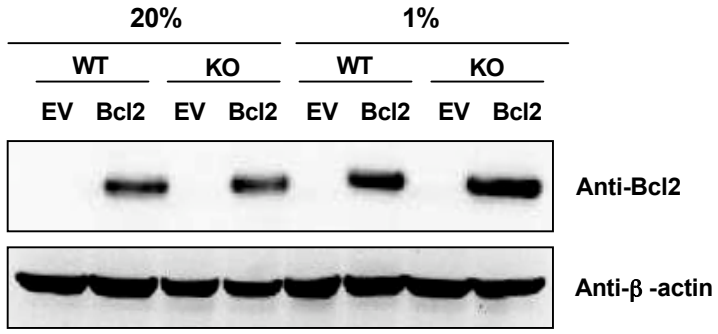
20%
1%
WT
KO
WT
KO
EV
Bcl2
EV
Bcl2
EV
Bcl2
EV
Bcl2
Anti-Bcl2
Anti-β -actin

S6

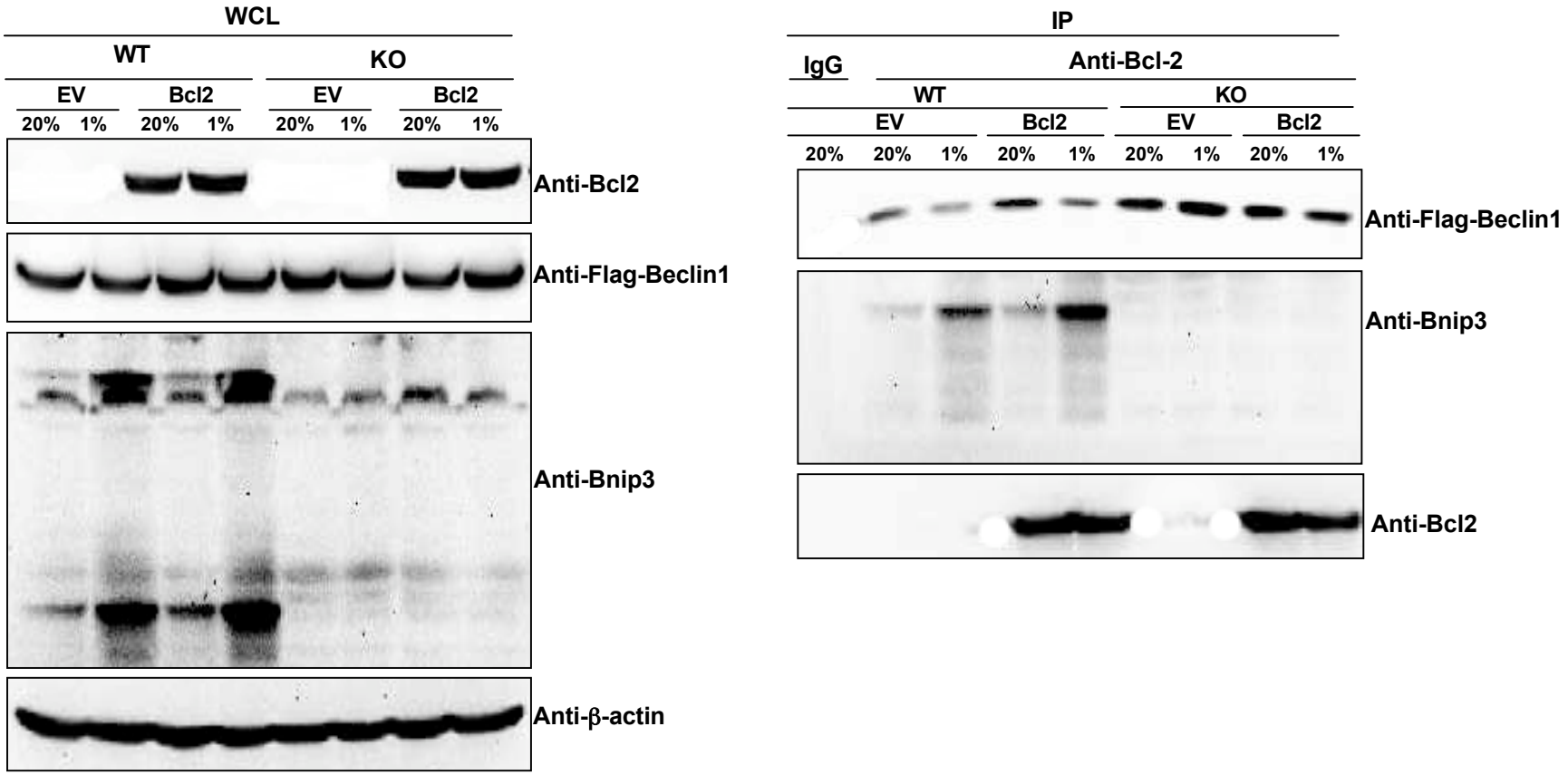
WCL
WT
KO
EV
Bcl2
EV
Bcl2
20%
1%
20%
1%
20%
1%
20%
1%
Anti-Bcl2
Anti-Flag-Beclin1
Anti-Bnip3
Anti-β-actin
IP
IgG
Anti-Bcl-2
WT
KO
EV
Bcl2
EV
Bcl2
20%
20%
1%
20%
1%
20%
1%
20%
1%
Anti-Flag-Beclin1
Anti-Bnip3
Anti-Bcl2

SUPPLEMENTAL FIGURE LEGENDS

Figure S1. Analysis of Mitochondrial DNA in Hearts of WT and HET mice DNA was extracted from the hearts of the same mice that were analyzed in Figure 1G. The mean (± SEM) levels of mitochondrial DNA relative to nuclear DNA were determined by quantitative real-time PCR. **P* < 0.05 by Student's *t* test compared to WT.

Figure S2. Analysis of Beclin-1 mRNA levels in MEFs with Beclin-1 Knockdown Total RNA was isolated from parental WT and KO MEFs (P) and subclones expressing a scrambled negative control shRNA (SNC) or shRNA targeted against Beclin-1 (shBeclin). Mean (± SEM) levels of Beclin-1 mRNA were determined by quantitative real-time RT-PCR. **P* < 0.05 by Student's *t* test compared to parental cells; $^{\#}$ *P* < 0.05 for indicated comparison.

Figure S3. Analysis of BNIP3 mRNA levels in MEFs with Beclin-1 Knockdown WT and KO MEFs, which were stably transfected with SNC or shBeclin short hairpin RNA, were cultured at 20% or 1% O_2 for 24 h, total RNA was isolated, and mean (± SEM) levels of BNIP3 mRNA were determined by quantitative real-time RT-PCR. **P* < 0.05 by Student's *t* test compared to WT-SNC at 20% O_2; $^{\#}$*P* < 0.05 by Student's *t* test compared to WT-SNC at 1% O_2.

Figure S4. Analysis of BNIP3 Protein Levels in MEFs with Beclin-1 Knockdown WT and KO MEFs, which were stably transfected with SNC or shBeclin short hairpin RNA, were cultured at 20% or 1% O_2 for 48 h, and cell lysates were subjected to immunoblot assays using antibodies against BNIP3 and β-actin as a loading control.

Figure S5. Analysis of Bcl2-overexpressing MEFs WT and KO MEFs that were stably transfected with empty lentiviral vector (EV) or a lentivirus encoding Bcl-2 were cultured at 20% or 1% O_2 for 48 h, and cell lysates were subjected to immunoblot assays using antibodies against Bcl2 and β-actin.

Figure S6. Analysis of Bcl2 Interaction with BNIP3 and Beclin-1 WT and KO MEFs that were stably transfected with empty lentiviral vector (EV) or a lentivirus encoding Bcl-2 were transiently transfected with an expression vector encoding FLAG-epitope-tagged Beclin-1 and cultured at 20% or 1% O_2 for 48 h. Whole cell lysates (WCL) were prepared. Aliquots of WCL were analyzed directly by immunoblot assays (left panel) or after immunoprecipitation (IP) with IgG or anti-Bcl2 antibodies (right panel).

Supplemental Table 1. shRNA information

Accession Number	Name	targeted sequence:
NM_009760	Mm Bnip3 sh80	5'-CAG CCT CCG TCT CTA TTT A -3'
	Mm Bnip3 sh82	5'- GCC TCC GTC TCT ATT TAT A -3'
NM_019584	shBeclin1	5'- CAG TTT GGC ACA ATC AAT A -3'

Supplemental Table 2. primer information

Accession No.	Name	Sense Primer	Anti-sense Primer
NC_005089	Mus musculus mitochondrion, ND2	CCCATTCCACTTCTGATTACC	ATGATAGTAGAGTTGAGTAGCG
NM_009760	Mus musculus BNIP3	ACTCAGATTGGATATGGGATTGG	GAGACAGTAACAGAGATGGAAGG
NM_019584	Mus musculus Beclin 1	AATCTAAGGAGTTGCCGTTATAC	CCAGTGTCTTCAATCTTGCC
NM_053069	Mus musculus Atg5	CCTGAAGATGGAGAGAAGAG	GGACAATGCTAATATGAAGAAAG

Mitochondrial Autophagy Is an HIF-1-dependent Adaptive Metabolic Response to Hypoxia

Huafeng Zhang, Marta Bosch-Marce, Larissa A. Shimoda, Yee Sun Tan, Jin Hyen Baek, Jacob B. Wesley, Frank J. Gonzalez and Gregg L. Semenza

J. Biol. Chem. 2008, 283:10892-10903.
doi: 10.1074/jbc.M800102200 originally published online February 15, 2008
